Title
SHIELDING AND ACTIVATION CONSIDERATIONS FOR A MESON FACTORY

Authors
Moyer, Burton J.
Wallace, Roger W.

Publication Date
1962-04-11

UCRL-10086

University of California

Ernest O. Lawrence Radiation Laboratory

Berkeley, California

DISCLAIMER

UCRL-10086

UNIVERSITY OF CALIFORNIA

Lawrence Radiation Laboratory
Berkeley, California

Contract No. W-7405-eng-48

SHIELDING AND ACTIVATION CONSIDERATIONS FOR A MESON FACTORY

Roger W. Wallace and Burton J. Moyer

April 11, 1962

SHIELDING AND ACTIVATION CONSIDERATIONS FOR A MESON FACTORY

Roger W. Wallace and Burton J. Moyer

Lawrence Radiation Laboratory
University of California
Berkeley, California

April 11, 1962

ABSTRACT

The shielding and activation of a meson factory are estimated by computing the emission spectra of the neutrons produced, and using these spectra to estimate the necessary shielding and the probable activation of the accelerator caused by the captured neutrons. The technique used in making these estimates is explained. It is assumed that a meson factory has an internal circulating beam current of 100μA of 450-, 600-, or 850-MeV protons. This beam will be assumed to hit an aluminum target of 100 g/cm^2.

SHIELDING AND ACTIVATION CONSIDERATIONS FOR A MESON FACTORY†

Roger W. Wallace and Burton J. Moyer

Lawrence Radiation Laboratory
University of California
Berkeley, California

April 11, 1962

1. Introduction and Method of Calculation

The calculation of the required shielding of a meson factory is of course the same as that for any other accelerator operating in the energy range of several hundred MeV. The only substantial difference is the considerably higher beam current of the factory, compared to previous accelerators. The special techniques used to achieve these higher beam currents do not have any bearing on the shielding or activation problem, and the experience gained in shielding cyclotrons in the same energy range is directly applicable. Since such an accelerator is fairly large physically and is quite expensive, the shielding is a major item in the budget. Also, it is not appropriate to use large safety factors for the shielding thickness, as might be done in the case of a small machine. As a result the necessary shielding thickness must be explored in greator detail than has sometimes been done in the past. In some cases shielding was sometimes relegated to the position of an afterthought or an accessory that could be added to a later date, when the initial construction expense of the accelerator itself was a few years in the past. The meson factory cannot be used effectively from its startup without the correct amount of shielding. The induced-activity problem presents an additional inconvenience in subsequent maintenancek and modification work. It also is a problem which must not be postponed until after construction.

---

† Work done under the auspices of the U. S. Atomic Energy Commission.

Unfortunately these problems are not of sufficient basic scientific interest, so that extensive calculations have been made with shielding primarily in mind. As a result each new estimate tends to be a more sophisticated, but still very appropriate, computation than the last, using the few basic references that are applicable to the problem. Perhaps some day very detailed Monte Carlo computations will be available, taking into consideration energy and angular distributions, and various geometrical situations in a more rigorous manner. Such calculations are now being initiated at the Oak Ridge National Laboratories in connection with the radiation-dose estimate for the project to send a man to the moon. These calculations are directed toward shielding against solar-flare protons but the lunar project is in many ways very similar to the meson factory shielding problem. The results, when available in a few years, will probably make the crude estimates of the type outlined herein out of date.

In the shielding of an accelerator in the several-hundred-MeV range the secondary neutrons, which are produced by the main-beam protons in the primary target and in the hardware of the accelerator, (themselves and the radioactivity which they induce) are the only important source of dose. By the time a sufficient thickness of shielding has been placed around the accelerator to attenuate the neutrons, the electromagnetic radiation and the charged particles have been very completely contained. The only known exception to this is that, in the very special case of much higher energy machines, in some special situations, μ mesons may be the controlling factor. Such will not be the case at meson-factory energies.

The technique generally used to estimate shielding is that developed by Moyer[1]. Each proton will produce a variety of particles as it undergoes collisions in the target and in the accelerator hardware. The greatest concentration of high-energy neutron secondaries is of course downstream from the target. With this exception, the secondaries are usually produced rather uniformly throughout the vacuum tank and pole faces of the magnet. At large distances from the accelerator the radiation pattern no longer shows much of this target-source origin. This problem has been extensively investigated by Patterson[2] and Dakin[3].

When protons strike an extended thick object the total neutron production as a function of energy for C, Be, Cu, and U are as shown in fig. 1. Thus we see that for an aluminum target, for the three energies we are considering, the total neutron production is given by table 1, which is derived in part from data of Moyer[4]). This total production consists of two parts. The "cascade" particles are knocked out during the immediate passage of the incident proton by direct interactions between it and individual nucleons in the target nucleus. These particles are strongly directed in the forward direction, and in general we will consider them to supply all the particles with energies above 150 MeV. The remainder of the secondary particles are, so to speak, "evaporated" from the nucleus at a later time by the general excitation energy which is left behind in it by the passage of the primary proton.

2. Cascades

The cascade process within individual nuclei is considered in detail in the Monte Carlo calculation by Metropolis et al.[5]). There has been some augmentation to allow for plural cascades within the target nucleus. The resulting yields of neutrons and protons from either neutron or proton bombardment is shown in fig. 2.

The synthesis of the overall neutron spectrum is from two parts:

(a) the cascade of neutrons above about 20 MeV and (b) the evaporation neutron spectrum, which is peaked in the few-MeV region. This synthesis is not only a natural approximation of this otherwise far too complex problem, but also, the use of these two parts of the spectrum in the evaluation of the problem represents a natural division. The cascade neutrons above 150 MeV are the only part of the spectrum that must be considered in the evaluation of the thickness of the shield. This is so because the lower energies have attenuation lengths that are substantially shorter than those for 150 MeV, and it is only this penetrating high-energy component

that controls the shield thickness. This can be seen in fig. 3, where there is a plateau in half-value thickness above about 150 MeV. There is of course a build-up and establishment of equilibrium spectrum in the first (inner) layers of the shield, but for practical shields of the thickness that will be needed for a meson factory, there is only the 46-cm half-value layer to be considered.

The spectrum of the cascade particles, computed by Metropolis et al.[5], is shown in fig. 4 for 460- and 1840-MeV incident protons. The spectra are seen to not differ by very much, except of course at the highest energies. These spectra, multiplied by the appropriate normalization factors given in table 1, are shown in the higher energy region of fig. 5. The angular distribution of the cascade particles is also secured from Metropolis et al.[5], but it has been augmented by Moyer[1], who used data from the Bevatron and from cosmic rays on the angular distribution of the prongs of nuclear stars in emulsion. This angular distribution is shown in fig. 6. The angular distribution is not sensitive to energy. The distribution is normalized for 6.2 GeV protons on Cu.

The work of Metropolis et al.[5] contains data on the net production of cascade nucleons at energies other than those of interest to meson factories—and for other target materials; and considerable additional information on the cascade process. Their technique is serving as a basis for the even more detailed computation now under way at Oak Ridge.

3. Evaporation

Several authors have treated the evaporation of nucleons from nuclei that have been excited by very high energy protons that will make up the low-energy end of our spectra[6–9]. Nuclear evaporation is somewhat analogous to the evaporation of a liquid on an atomic scale. The resulting particle spectra are obtained by estimating an excitation energy E_1 for the nucleus as a whole. This estimation, due to Moyer[4], is shown in detail for Ne and Al in fig. 7. The excitation energy is related to

the square of the nuclear temperature by an empirical parameter (A/10) due to Dostrovsky[6]):

$$E_1 = \left(\frac{A}{10}\right) \tau^2 \qquad (1)$$

where E_1 = the nuclear excitation in MeV, A = the atomic number of the nucleus, A/10 = the empirical parameter having the dimensions MeV^{-1}, and τ = the nuclear temperature (MeV). The resulting nuclear temperatures for Ne and Al are shown in fig. 8. The evaporation spectrum itself is then given by

$$N(E)dE = \left(\frac{E}{\tau^2}\right) e^{-(E/\tau)}\, dE. \qquad (2)$$

The E in front of the exponential, instead of the usual $E^{1/2}$ which appears in the Maxwellian energy distribution, is necessary to account for higher velocity nucleons escaping from greater "depths" in the nucleus in a manner analogous to the same relation for the energy distribution in a molecular beam emerging from an oven.

In order to estimate the complete spectrum it is now necessary to fit together this Maxwellian low-energy evaporation end and the Metropolis high-energy "tail." This fit is made after each individual spectrum has been normalized to the estimated total production of its particular component, as given in table 1. This relation is shown as a function of the bombarding energy for both neutron and proton evaporation products in fig. 9. More details of this process are available, such as the suppression of the low energies by the Coulomb barrier—as treated by Le Couteur[7]) and Deutsch[9]). Heavier particles such as H^2 and H^3, as well as multiply charged particles such as He^3 and He^4, can be estimated. The doubly charged particles have their evaporation spectrum peaks at about twice the energy of the proton spectrum peak from a nucleus with the same excitation temperature.

The angular distributions of the evaporation particles, by the very meaning of evaporation, are of course isotropic. The evaporation particles produced in the target have no chance of penetrating the main shields directly, as has been explained. Therefore, they are mainly of interest with regard to the radioactivities they induce in the hardware of the accelerator. They are more important in this activity production than the cascade neutrons, because their energy is more favorable and they are more numerous. More extensive data on evaporation particles is given by Moyer[4]). The smooth fit of the two parts of the spectra shown in fig. 5 has only been done by eye. Greater accuracy is not appropriate to the problem.

4. Shield Attenuation

The thick shields required around accelerators provide their neutron attenuation by absorbing, degrading, or deviating the neutrons by nuclear collisions. At the high energies of the cascade particles, elastic scattering is so strongly peaked in the forward-directed diffraction patterns that essentially no deviation or energy loss occurs. Thus as the neutron energy is increased from the evaporation region to the cascade region the effective removal cross section for neutrons in the shield decreases from the total cross section to the inelastic cross section.

This effect is shown in tables 2, 3, and 4, from Patterson[2]), as applied to the elements present in concrete. It is seen that $N\sigma_a(cm^{-1})$ is a figure of merit for the efficiency of each element. Table 4 emphasizes the importance of the heavier elements as the neutron energy is raised. Points calculated from these data by Patterson[2]) are plotted in fig. 10, together with several experimental values for energies from 1 MeV to 4.5 GeV. The agreement is quite good. The same data appear in a transposed form in c. g. s. units in fig. 3. The data only apply to thick shields and poor-geometry situations.

The measurements of σ_{total} and $\sigma_{reaction}$ for various nuclei as a function of neutron energy up to 5 GeV are given by Coor et al.[10]) and Atkinson et al.[11]), and are shown in Lindenbaum[12]). This experimental work shows that the attenuation of neutrons in the high energy region is essentially constant.

5. Radiation Emerging From the Shield

Now that the spectrum and angular distribution of the neutrons produced in the target and accelerator hardware by the primary protons, both in the beam and lost from it at the end of acceleration, have been estimated, a secondary calculation can be made of the penetration of the outer shield by these neutrons. This can be done by using similar data for cascade particles produced by neutrons, secured from the same sources as that given earlier for incident protons. The pertinent cascade and evaporation data per incident neutron are given in table 5, taken from Moyer[1]). The evaporation data are the same as those for incident protons, whereas the cascade values are not. In order to emphasize this comparison the data for protons incident on atomic weight A = 20(Ne) are shown in table 6. As would be expected, the neutrons are more numerous in neutron-induced cascades than in proton-induced cascades, and vice versa for proton-induced cascades. The above-mentioned tables also include cascade mesons, which gradually increase in importance from 500-MeV incident energy on up. They do not, as mentioned earlier, become a controlling factor in the energy range considered form meson factories.

Table 7, which contains data for targets of atomic weight A = 60, is included to make it possible to interpolate for the intermediate elements present in shielding, as has been done in the case of aluminum, in figs. 7 and 8. Also included in the evaporation part of tables 6 and 7 are the numbers of other atomic species such as H^2, H^3, He^3, He^4, and Li, Be, C, etc., which are evaporated in addition to the neutrons and protons at higher excitation values in lesser amounts.

The flux of particles present on the outside of the shield now consists of the directly transmitted primary neutrons of energy > 150 MeV from the spectra of fig. 5, plus a contribution of evaporation fragments produced by these high-energy neutrons that suffer inelastic collisions in the outer layers of the concrete shield. The data in table 5 for A = 20 should be used with care for other values of A, because higher values of A give much larger evaporation neutron yields, and elements with higher values of A — such as Si and Ca — are an important part of the concrete shield wall.

The number of primary target neutrons making inelastic collisions within an outer layer of the shield wall of thickness x is

$$N = M\,(e^{x/\lambda} - 1), \qquad (3)$$

where x is measured in from the outside of the shield, and λ is the mean free path for inelastic collisions of the neutrons. Assume that half of these evaporation neutrons emerge. This is an obvious over-estimate, but it will to some extent be compensated for by the further multiplication of some of the cascade neutrons in secondary collisions of their own before emerging on the outside of the shield. None of the protons produced in the aluminum target will emerge from the outside of the shield because of range limitations. There will, however, be protons emerging from the outside of the shield, arising from the evaporation processes produced as outlined above.

Considering an outer layer of the shield $x = \lambda$, one mean free path thick, for cascade production; and using the spectra of fig. 5, the data in table 5, and values of λ shown in fig. 17 from Lindenbaum[12]; we estimate that each primary neutron that passes through the outer shield will be accompanied by 0.6 fast neutrons and 0.3 protons.

There will also be a small flux of thermal neutrons and gamma rays. The gammas come from thermal neutron capture by the H of the shield and also from nuclear deexcitations associated with evaporation processes. Typically, the numerical value of the thermal neutron flux is only a few times that of the fast neutrons, so the relative dosage from the thermal sections is negligible, taking RBE values into account, in comparison with the fast neutrons. Ionization-chamber measurements of the gamma-ray dosage are typically one-quarter or less than that arising from fast neutrons.

6. Propagation of Radiation to Distant Locations

The propagation of the emitted radiation from the outside of the shielding to distant locations has been treated theoretically by Moyer[1], and experimentally by Patterson[2] and Dakin[3]. Two processes of propagation are involved. First, there is direct flight of the higher-energy cascade and more energetic evaporation components with inverse-square and exponential attenuation by air collisions. Second, there is diffusion of the lower-energy evaporation components. These processes will be treated in three parts.

6.1 DIFFUSION OF EVAPORATION NEUTRONS

The solution of the Boltzmann diffusion equation

$$\nabla^2\phi - \frac{\phi}{L^2} = \frac{1}{r}\,\frac{d^2(r\phi)}{dr^2} - \frac{\phi}{L^2} = 0 \qquad (4)$$

for a point source of monoenergetic neutrons and a spherical geometry of surrounding medium with uniform scattering and capture cross section is:

$$\phi(r) = \phi_1\,\frac{r_1}{r}\,e^{\left[-(r-r_1)/\sqrt{\lambda_a \lambda_{tr}/3}\right]}, \qquad (5)$$

where

$\phi(r)$ = the flux density at the distance r from the source,

ϕ_1 = the flux density at the distance r_1 from the source,

λ_a = the mean free path for absorption of the neutrons,

λ_{tr} = the transport mean free path,

$\sqrt{\lambda_a \lambda_{tr}/3}$ = the characteristic length in the diffusion equation.

If the Boltzmann diffusion equation had been solved for the case of a medium in which the characteristic collision mean free path is very long, the distance dependence would be, for the i^{th} energy group:

$$\phi_i(r) = \frac{A_i}{r_i^2} e^{-(r/\lambda_i)} , \qquad (6)$$

where A_i is the source strength per steradian in a particular direction for neutrons with collision mean free path λ_i. Values for λ_i are given for several energies in the column labeled $\lambda_{collision}$ of table 8. In the case of the diffusion process described by eq. (5), the distance dependence is an exponential attenuation multiplied by $1/r$ whereas in the case of direct flight with attenuation, described by eq. (6), $1/r^2$ appears instead. Thus the radial fall-off of flux intensity is less rapid in the case of diffusion.

We will assume in the diffusion case that at the outer shield surface, taken to be at a distance of 10 m from the center of the accelerator the low-energy evaporation neutrons have achieved a random direction and are properly described by eq. (5). It has been estimated by Moyer[1]) that ϕ_1 is 1.7 times the surviving number of primary target neutrons penetrating the sphere at the radius r_1 = 10 m. This function, with 250 meters substituted in the exponent, is plotted in fig. 11. The diffusion of neutrons has also been treated by Lindenbaum[12]), using slightly different parameters.

6.2 SURVIVING PRIMARY TARGET NEUTRONS OF ENERGY GREATER THAN 150 MeV

Expressing A_i in eq. (6) as a function of the angle $F_0(\theta)$ target yield per steradian; substituting the collision mean free path for neutrons above 150 MeV; and multiplying by an attenuation exponential for the shield, of thickness t, we have:

$$F(r,\theta) = \frac{F_0(\theta)}{r^2} e^{-(t/\lambda_{sh})} e^{-(r/740)}, \qquad (7)$$

where λ_{sh} is the mean free path for removal in the shielding. If directions are being considered that intersect the magnet iron, then an additional exponential for that can be multiplied in. This flux is plotted in fig. 11. It is seen that the curves for A and B categories are too close together and too parallel to be distinguished easily in the region out to several hundred meters. Beyond this distance the fluxes are too small for accurate measurements. At the present time it is not known whether A or B is the dominant process, but clearly some of each is involved since varying azimuthal dependence is experimentally observed in addition to what is closely a $1/r^2$ dependence, as seen in the data of Patterson[2] in fig. 12.

6.3 DIRECT FLIGHT OF CASCADE AND EVAPORATION NEUTRONS FROM THE OUTER SURFACE OF THE SHIELD.

These neutrons are produced in the outer layers of the shield—not at the center of the accelerator in a point source. As a result some additional geometric assumptions must be made. Moyer[1] has assumed that one steradian of solid angle is available to the cascade neutrons and that their diffusion can be considered to come from point sources located on the outside of the shielding. This gives a flux density for the secondary neutrons of the $\underline{i}^{th}$ energy group:

$$F_s^{\,i}(r,\theta) = F_0(\theta)\, e^{-(t/\lambda_{sh})} \frac{1}{4\pi} \left[B^i/(r-r_s)^2 \right] e^{-\left[(r-r_s)/\lambda_i\right]}, \qquad (8)$$

where

$r - r_s$ = the distance of the observation point from the outer surface of the shield,

B^i = the number of emerging secondary neutrons in energy group i accompanying each emerging primary neutron.

7. Activation

The thermal flux inside the shielding can be estimated quite well by the relation:

$$\phi_{th} = 1.25 \frac{Q}{S} \qquad (9)$$

which is described by Patterson[13], where Q fast neutrons are released into the accelerator vault per second, and the inside surface area of the vault is S cm^2. The spectrum of the neutrons in the process of degradation is approximated by assuming each emission increment $Q(E_1)\Delta E_1$ to give rise to a flux increment with spectrum $1/E - 1/E_1$. Thus, by integration, the "slowing down" flux has the spectrum:

$$\phi(E) = K_1 \int_E^{E_{max}} Q(E_1) \left(\frac{1}{E} - \frac{1}{E_1} \right) dE_1 . \qquad (10)$$

This "slowing-down" flux spectrum is joined by continuity of slope to the thermal spectrum

$$\phi_{th} = K_2 E^{1/2} e^{-(E/kT)}, \qquad (11)$$

which in turn is normalized by requiring the integral from zero energy to 0.5 eV to give the value 1.25 Q/S given in eq. (9).

Although much has been written about the induced activities in the vaults of accelerators[14, 15, 16], and there is a good understanding of the observed radiation levels, it is probably best to extrapolate the measurements made with the 184-inch cyclotron at Berkeley to the proposed meson factories. After many years of

operation with 1 μA of 340-MeV protons and 180-MeV deuterons, the induced radioactivity inside the vault as a function of the time after shutdown was characteristically shown in fig. 13. The four prominent half-lives are identified. The mean radiation level after several days of decay is about 2 mr/hr. Since these measurements were made, the cyclotron has been converted to accelerate 730-MeV protons—on which it operates about 70% of the time. The remainder of the time is spent accelerating 450-MeV deuterons and 900-MeV alpha particles. Boom[15] has measured the spectrum of gamma rays in the vault after extended operation with 730-MeV protons. He found that the mean radiation level after 48 hr of shutdown is about 10 mr/hr. The main activity that he observed in the magnet gap was Co^{58}.

Boom concluded that an 850-MeV meson factory operating at 100 μA would have a serious induced-activity problem. Table 9 shows the total neutron yield from a copper target when struck by a variety of particles which have been or might be accelerated in the LRL cyclotron plus the two meson factory energies of 450 and 600 MeV. It is seen that by extrapolating from our many years of operating experience with 340-MeV protons to 100 times the beam, with 850-MeV protons, the induced background in the vault after about 48 hours of shutdown—is raised by a factor of 500. That is, from 2 mr/hr to 1 r/hr—which makes working intolerable. If one extrapolates from the 730-MeV levels, the increase is by a factor of 100 to 1 r/hr.

Boom[15] suggests that two steps be taken to alleviate this dire situation: First, use as much aluminum and as little stainless steel as possible. This suggestion has often been made, but experiments made at the Bevatron, 184 and 60-inch LRL cyclotrons indicate that the use of aluminum is unwise. Even several weeks after shut down aluminum is the most radioactive metal at the Bevatron. It seems unlikely that any large advantage is to be gained from the substitution of one common construction material for another. However, Boom's second suggestion, shielding against the long-lived activities, which are mainly 510- and 810-keV Co^{56} and Co^{58} gammas, is not difficult and would probably be effective.

To reduce these gammas by an order of magnitude requires 2 cm of lead. Such shields could probably be installed locally and would make it possible to preform brief maintenance work several days after shutdown—with, of course, considerable inconvenience, compared to present practice. Certainly all equipment that does not actually have to be located in the accelerator vault should be located on the floor below or removed completely from the shielded area. The vault floor should be made thick enough so that the equipment located below will not itself become radioactive to a serious degree.

8. Conclusion and Summary

The production of neutrons in a meson-machine target due to the cascade and evaporation processes has been described, and spectral and production estimates made. The subsequent production of secondaries in the shield wall has been treated. The neutron atmosphere inside the accelerator vault, which is responsible for the induced activity of the accelerator hardware, was estimated (Sec. 7). It was concluded that 35 ft of concrete in the forward direction from the target would allow industrial occupancy of a point 50 ft from the target. Of course dense concrete could reduce these dimensions in the inverse ratio of the densities. The induced-activity problem is not as easily solved, and immediate access to the vault after shutdown is out of the question. However, local shielding can help in the performance of brief maintenance jobs a few days after shutdown.

Acknowledgments

The authors especially wish to thank personnel at the Laboratory who have given valuable assistance; specifically, H. W. Patterson and A. Smith of the Health Physics group and E. L. Kelly of the 88-inch cyclotron.

REFERENCES

1) B.J. Moyer, Method of Calculation of the Shielding Enclosure for the Berkeley Bevatron, in First International Symposium on Protection Near Large Accelerators, Saclay, January 1962 (to be published).

2) H. Wade Patterson, The Effect of Shielding on Radiation Produced by the 730-MeV Synchrocyclotron and the 6.3-GeV Proton Synchrotron at the Lawrence Radiation Laboratory (UCRL-10061, Jan. 1962); in First International Symposium on Protection Near Large Accelerators, Saclay, Jan. 1962 (to be published

3) H.S. Dakin (Lawrence Radiation Laboratory, Berkeley), private communication.

4) B.J. Moyer, Data Related to Nuclear Star Production by High-Energy Protons, Lawrence Radiation Laboratory, June 20, 1961 (unpublished).

5) N. Metropolis, R. Bivins, M. Storm, A. Turkevich, J.M. Miller, and G. Friedlander, Phys. Rev. 110 (1958) 185; and 110 (1958) 204.

6) I. Dostrovsky, P. Robinowitz, and R. Bivins, Phys. Rev. 111 (1958) 1659.

7) K.J. Le Couteur, Proc. Phys. Soc. (London) A63 (1950) 259.

8) Y. Fujimoto and Y. Yamaguchi, Prog. Theoret. Phys. (Kyoto) 4, 468; 5, 76; and 5, 787 (all in 1950).

9) R.W. Deutsch, Phys. Rev. 97 (1955) 1110-23.

10) T. Coor, D.A. Hill, W.F. Hornyak, L.W. Smith, and G. Snow, Phys. Rev. 98 (1955) 1369.

11) J.H. Atkinson, W.N. Hess, V. Perez-Mendez, and R. Wallace, Phys. Rev. 98 (1955) 1369.

12 S.J. Lindenbaum, Shielding of High-Energy Accelerators, in Ann. Rev. Nuclear Sci. 11 (1961) 213.

13) H.W. Patterson and R. Wallace, A Method of Calibrating Slow-Neutron Detectors, Lawrence Radiation Laboratory Report UCRL-8359, July 1958 (unpublished).

[14] B. J. Moyer, Shielding and Radiation Calculations for USNRDL Cyclotron, Lawrence Radiation Laboratory, October 11, 1960 (unpublished).

[15] R. W. Boom, K. S. Toth, and A. Zucker, Residual Radiation of the LRL 184-Inch Cyclotron, Oak Ridge National Laboratory Report ORNL-3158, July 1961 (unpublished).

[16] W. Wadman, 184-Inch Synchrocyclotron--Decay of Induced Activities, Lawrence Radiation Laboratory, November 13, 1961 (unpublished).

FIGURE CAPTIONS

Fig. 1. Estimated thick-target neutron yields from proton bombardment.

Fig. 2. Estimated cascade neutrons and protons produced by incident neutrons or protons of energy E_n on nuclei near $A = 20$.

Fig. 3. Half-value reduction thickness for high-energy neutrons in ordinary concrete.

Fig. 4. Energy spectra of cascade nucleons emitted from aluminum.

Fig. 5. Cascade and evaporation neutron emission spectra from 450-, 600-, and 850-MeV protons on aluminum.

Fig. 6. Angular distribution of neutrons, over 150 MeV in energy, from a single collision in Cu by 6.3-GeV protons (normalized to 8 neutrons/proton).

Fig. 7. Nuclear excitation energy E_i produced by incident neutron or proton of energy E_n in nuclei with A near 20.

Fig. 8. Estimated residual nuclear temperature after excitation by a neutron or proton of energy E_n for an element near $Z = 20$.

Fig. 9. Estimated evaporation neutrons and protons produced by incident neutrons or protons of energy E_n on nuclei near $A = 20$.

Fig. 10. Attenuation of neutrons in ordinary concrete. At 90 and 270 MeV, measurements were made at the 184-inch 340-MeV cyclotron. At 4.5 GeV the measurement was made at the Bevatron.

Fig. 11. Comparison of radial dependence of neutron fluxes from high-energy direct flight and low-energy diffusion.

Fig. 12. Fast neutron flux measured with cadmium-paraffin-indium detectors at different distances from the Bevatron.

Fig. 13. Radiation intensity near 184-inch cyclotron tank vs time after shutdown (340-MeV protons, 1 μA, for several hours). The Fe^{59} (45 days) and Mn^{54} (300 days) are not resolved.

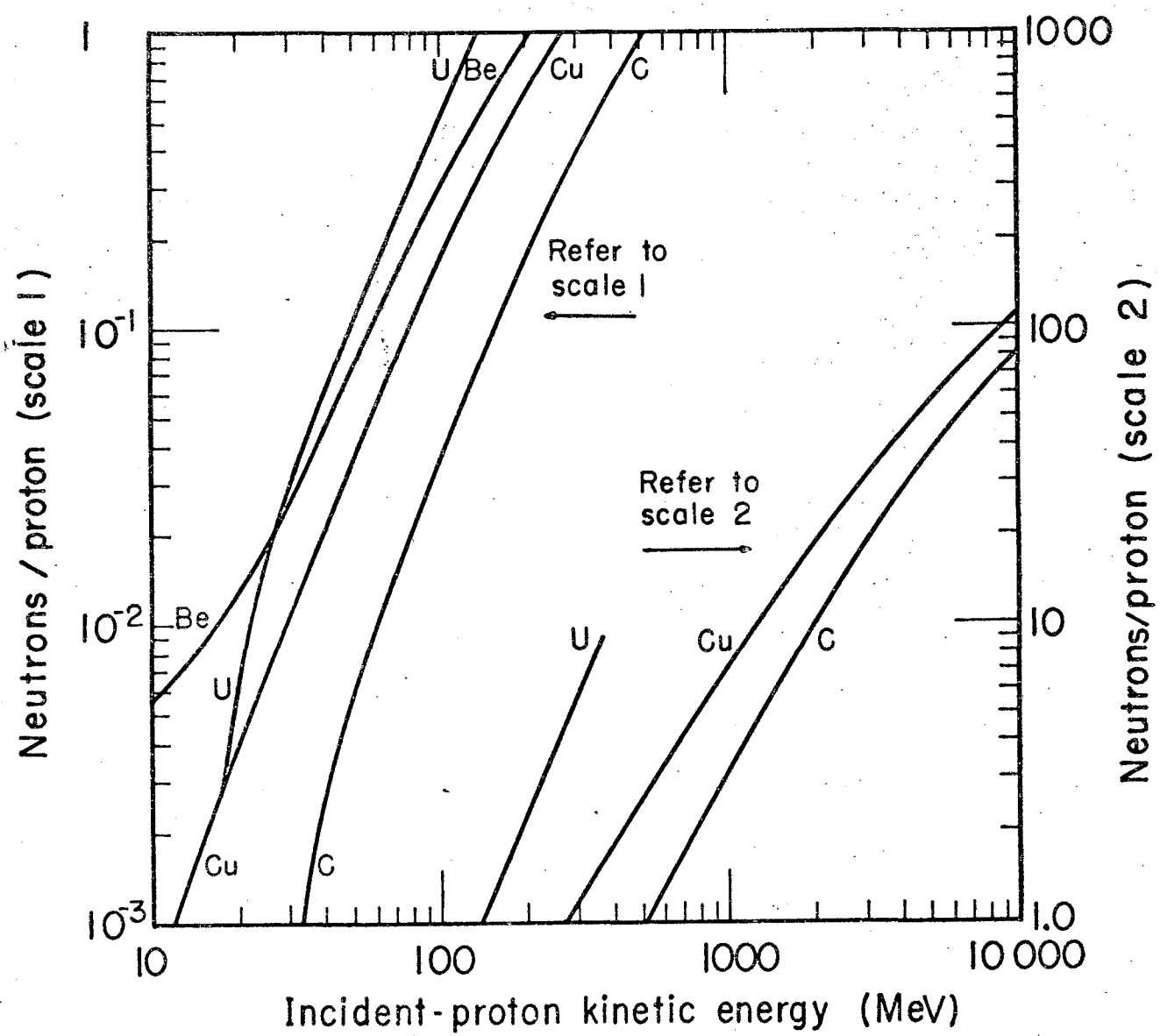

MU-25446
UCRL-10086
Fig. 1

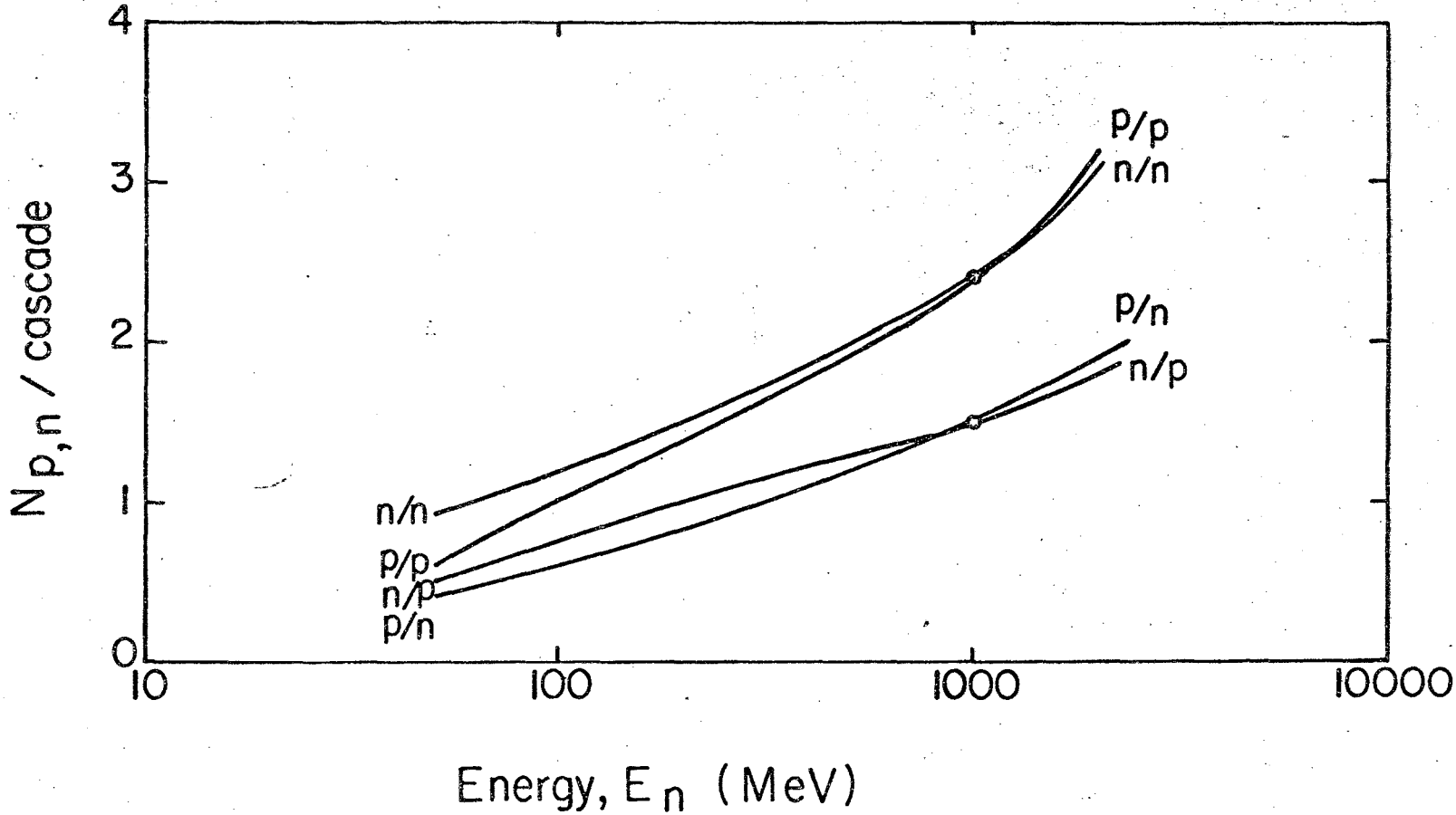

MU-26623
UCRL-10086
Fig. 2

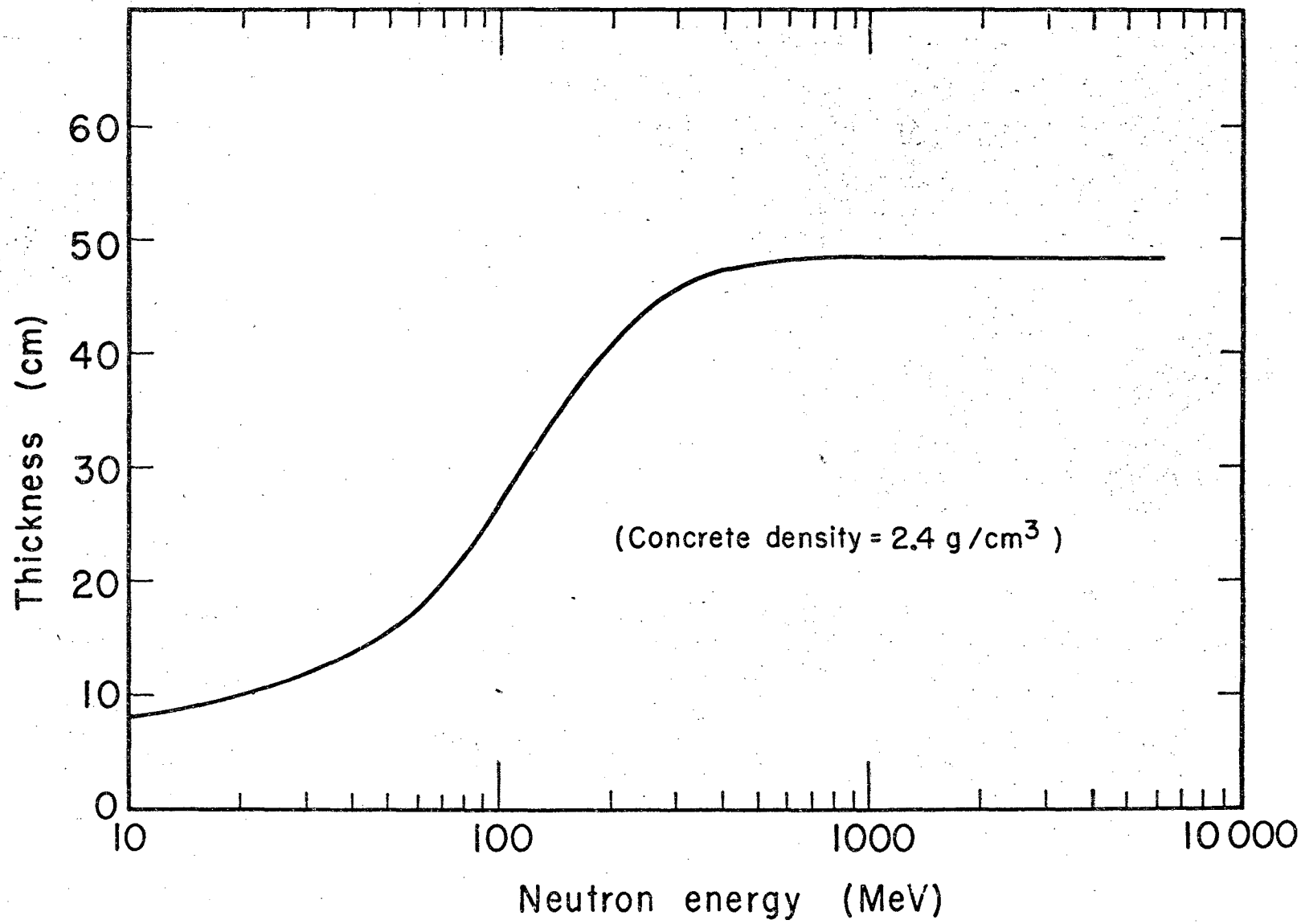

MU-25447
UCRL-10086
Fig. 3

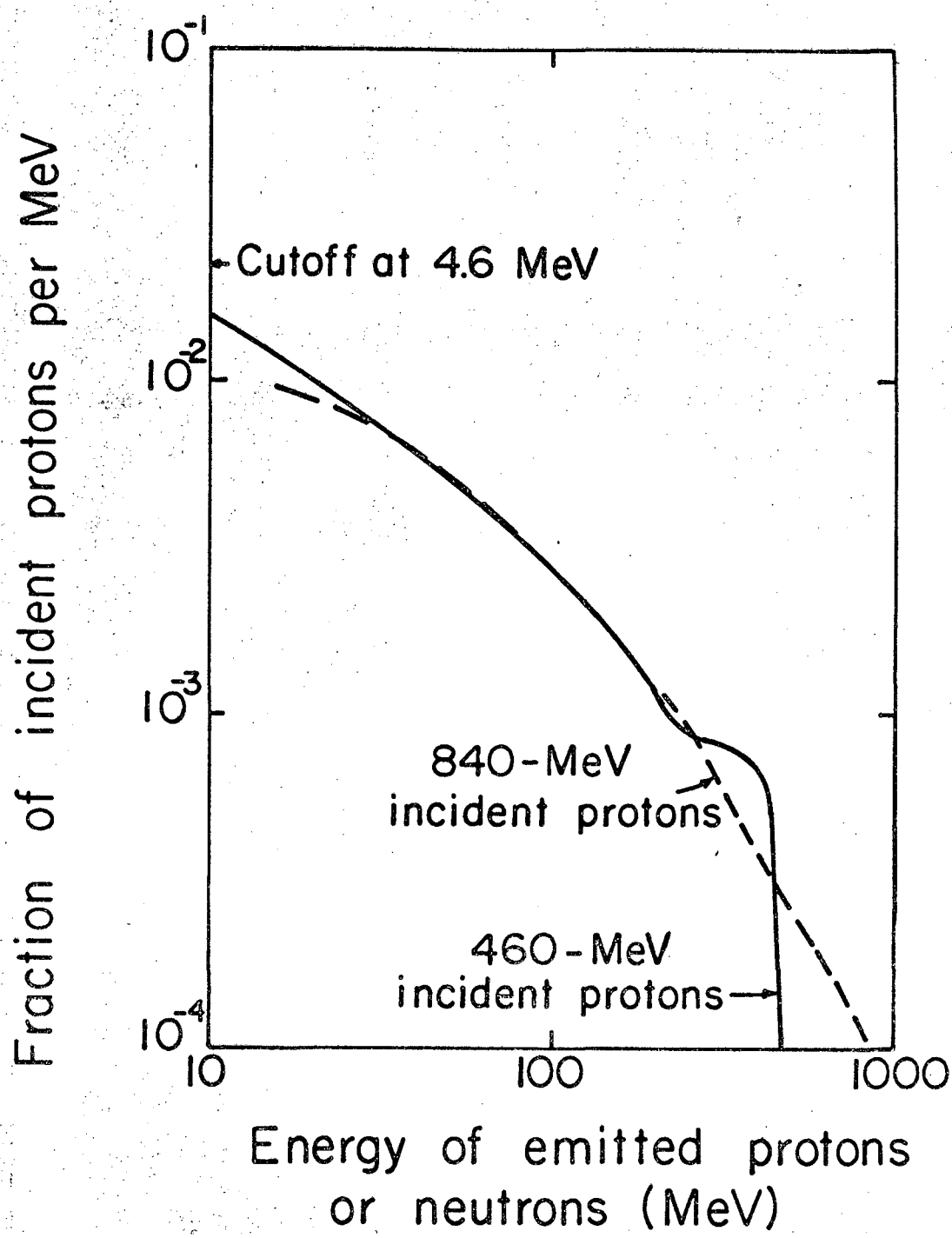

MU-26624
UCRL-10086
Fig. 4

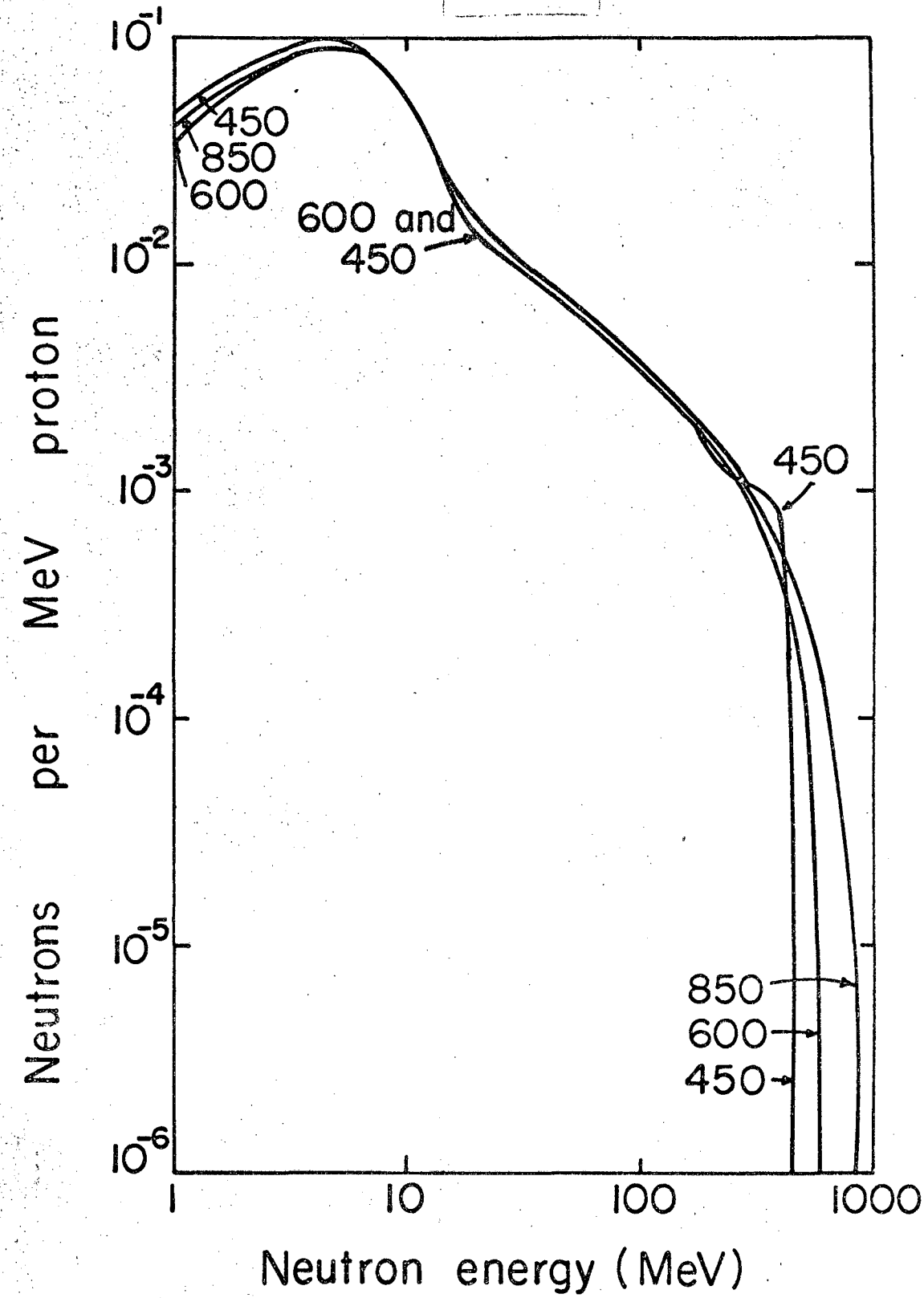

MU-26625
UCRL-10086
Fig. 5

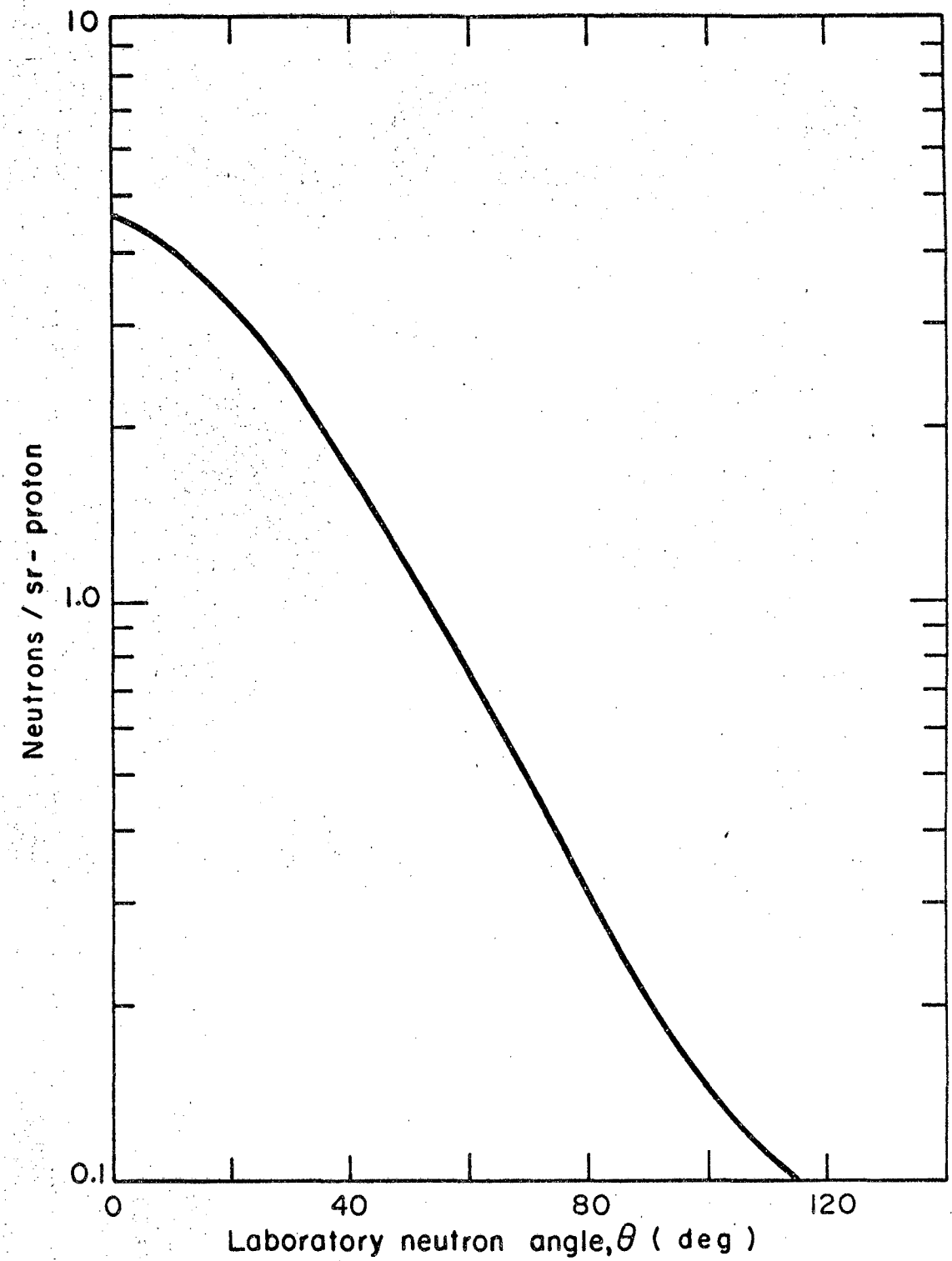

MU-24266
UCRL-10086
Fig. 6

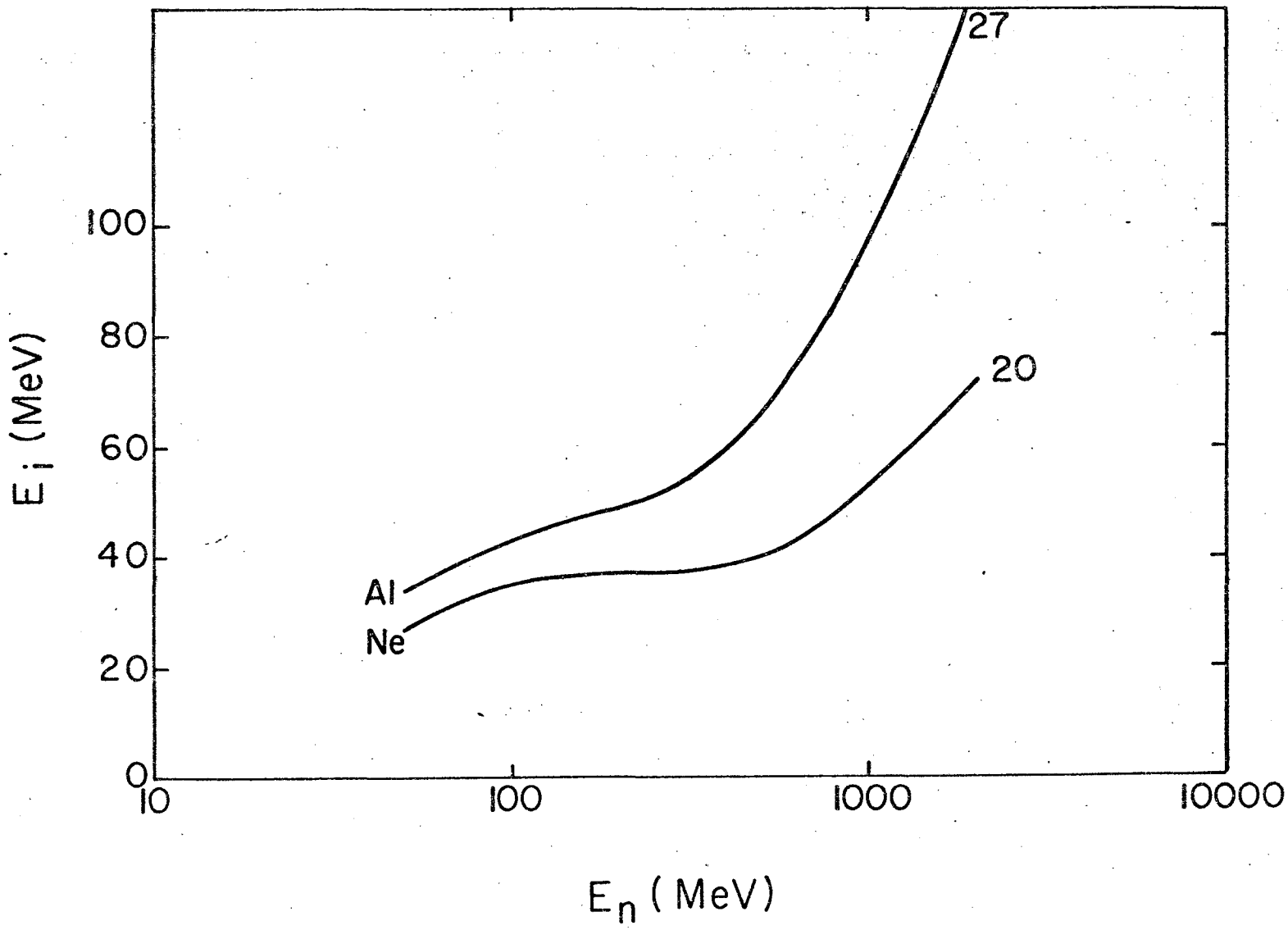

MU-26626
UCRL-10086
Fig. 7

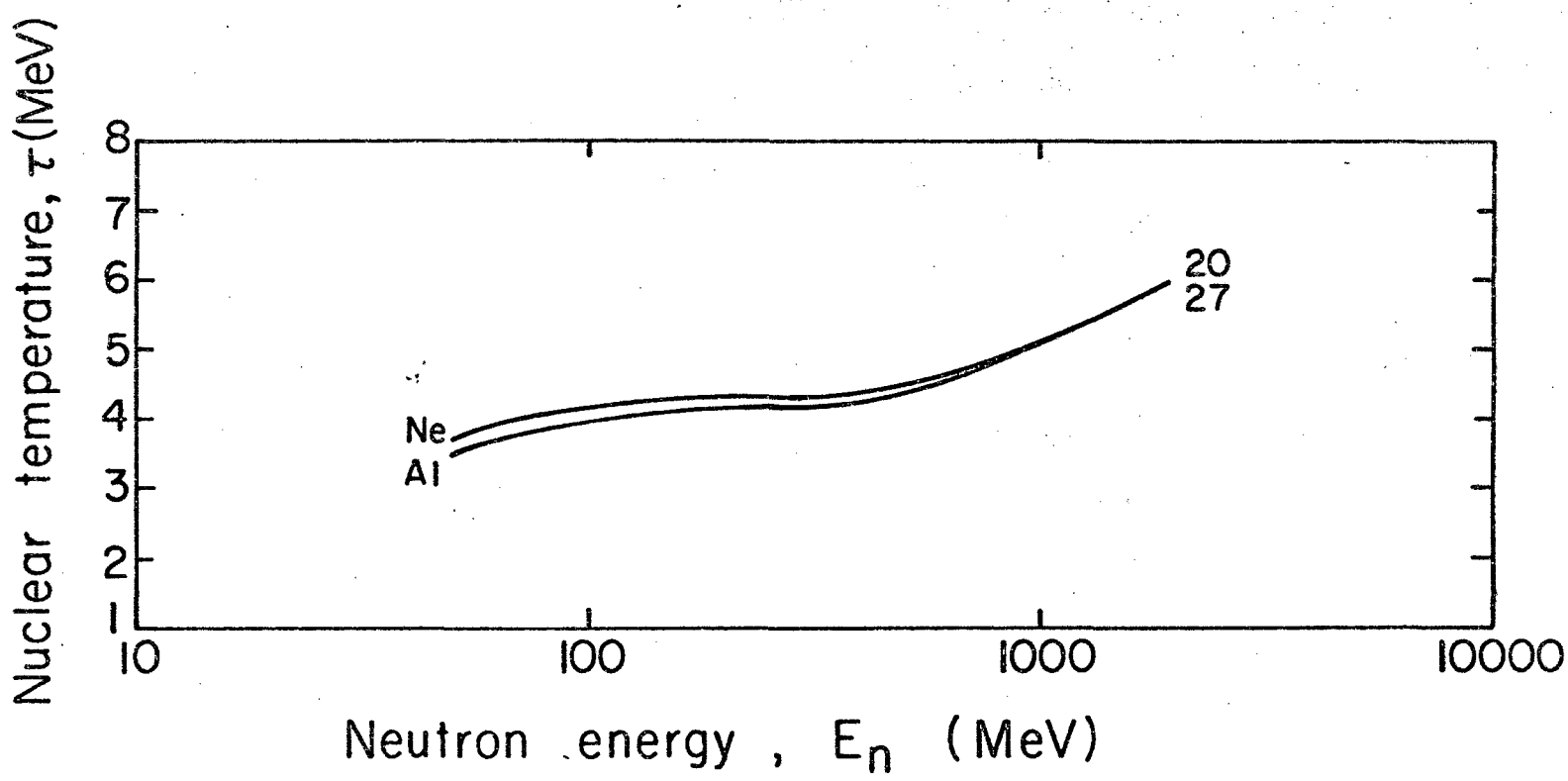

MU-26627
UCRL-10086
Fig. 8

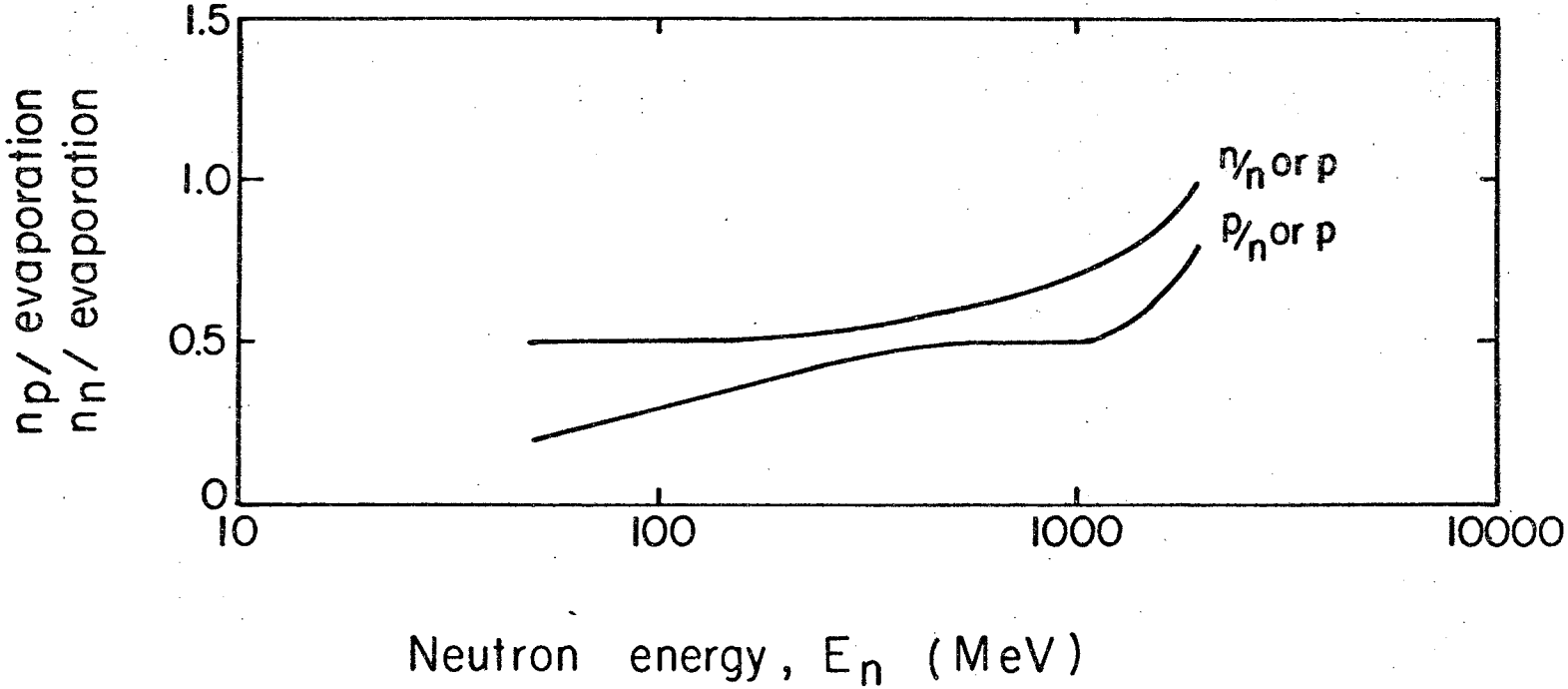

MU-26628
UCRL-10086
Fig. 9

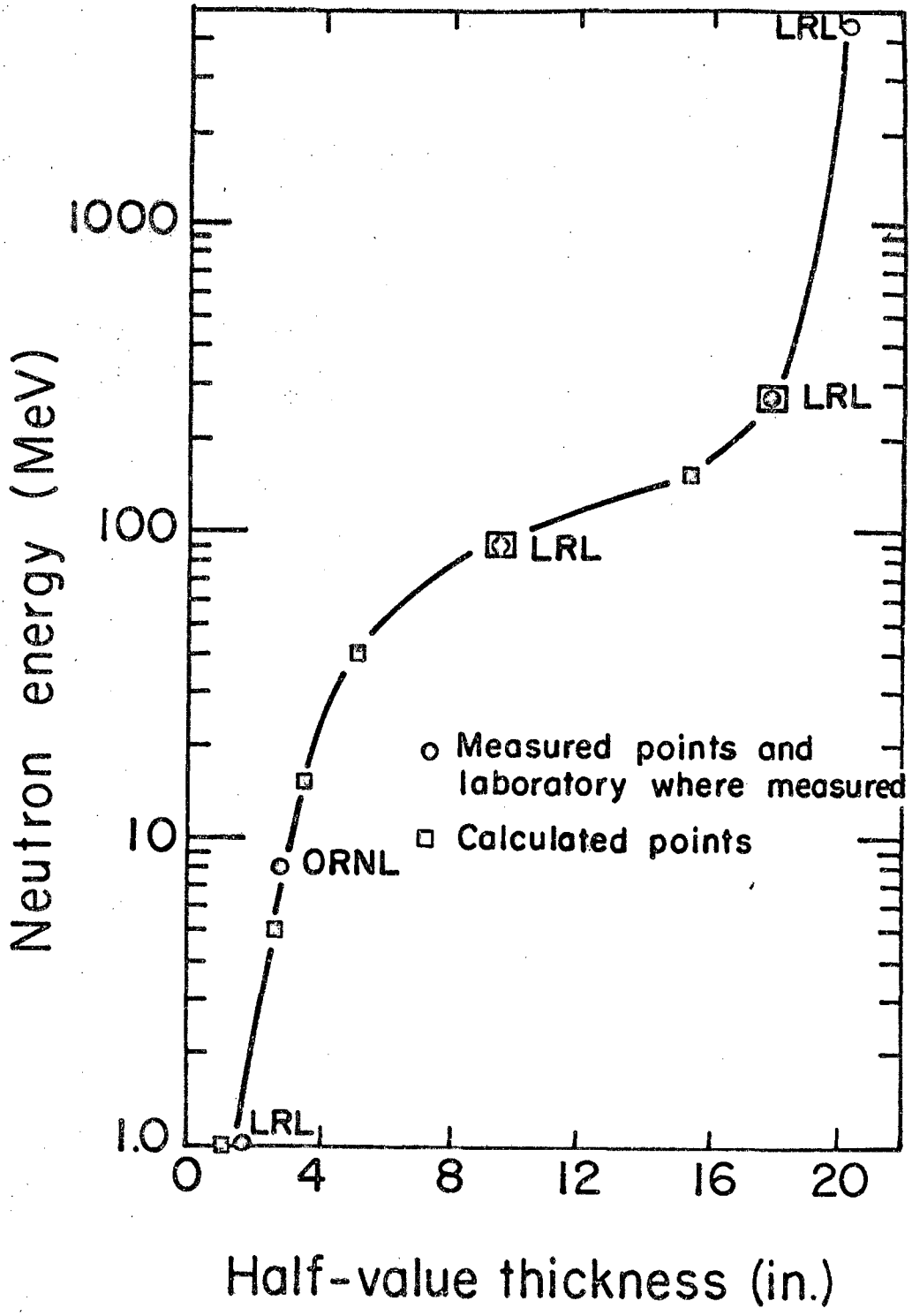

MU-26629
UCRL-10086
Fig. 10

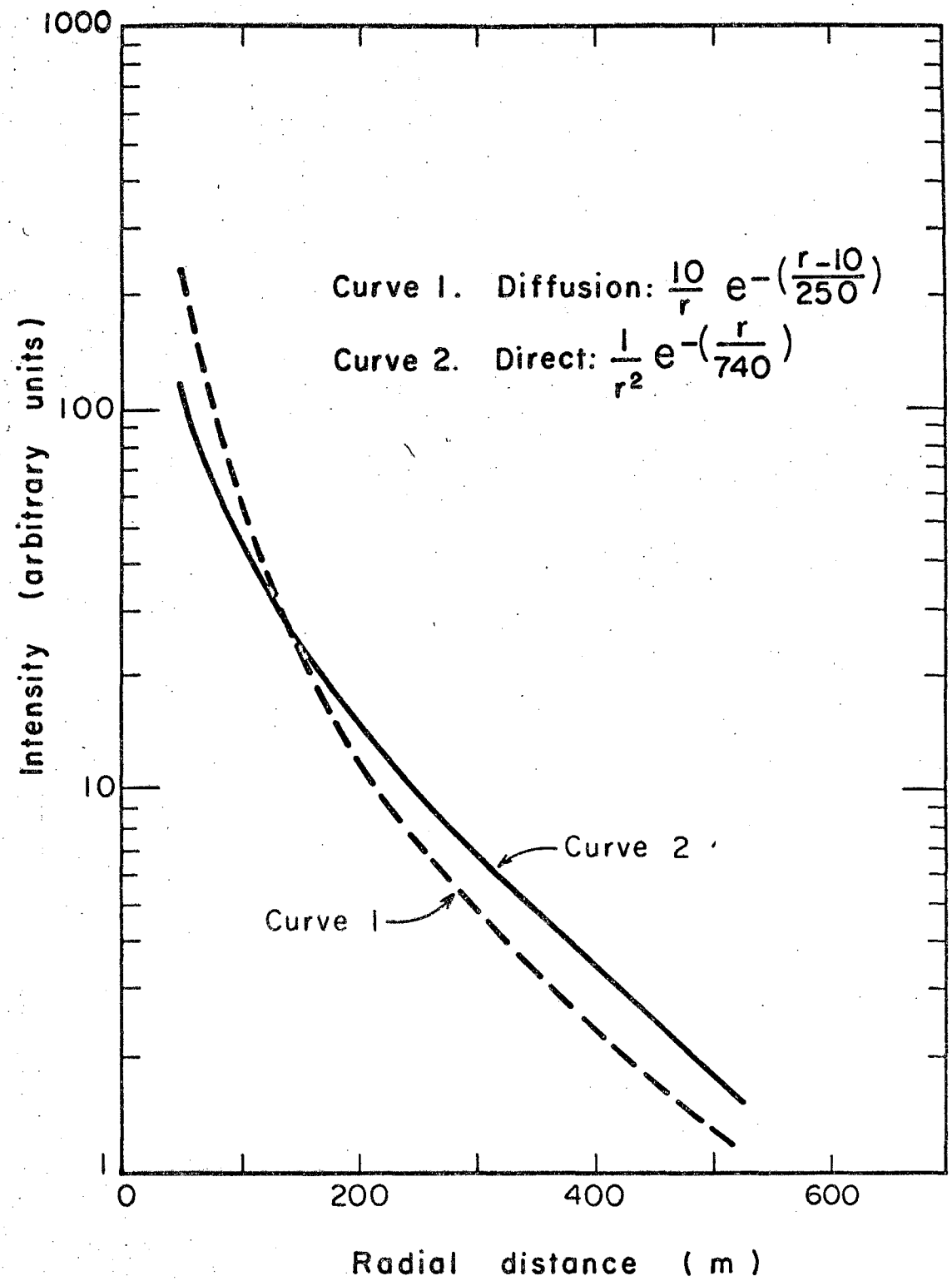

MU-25474
UCRL-10086
Fig. 11

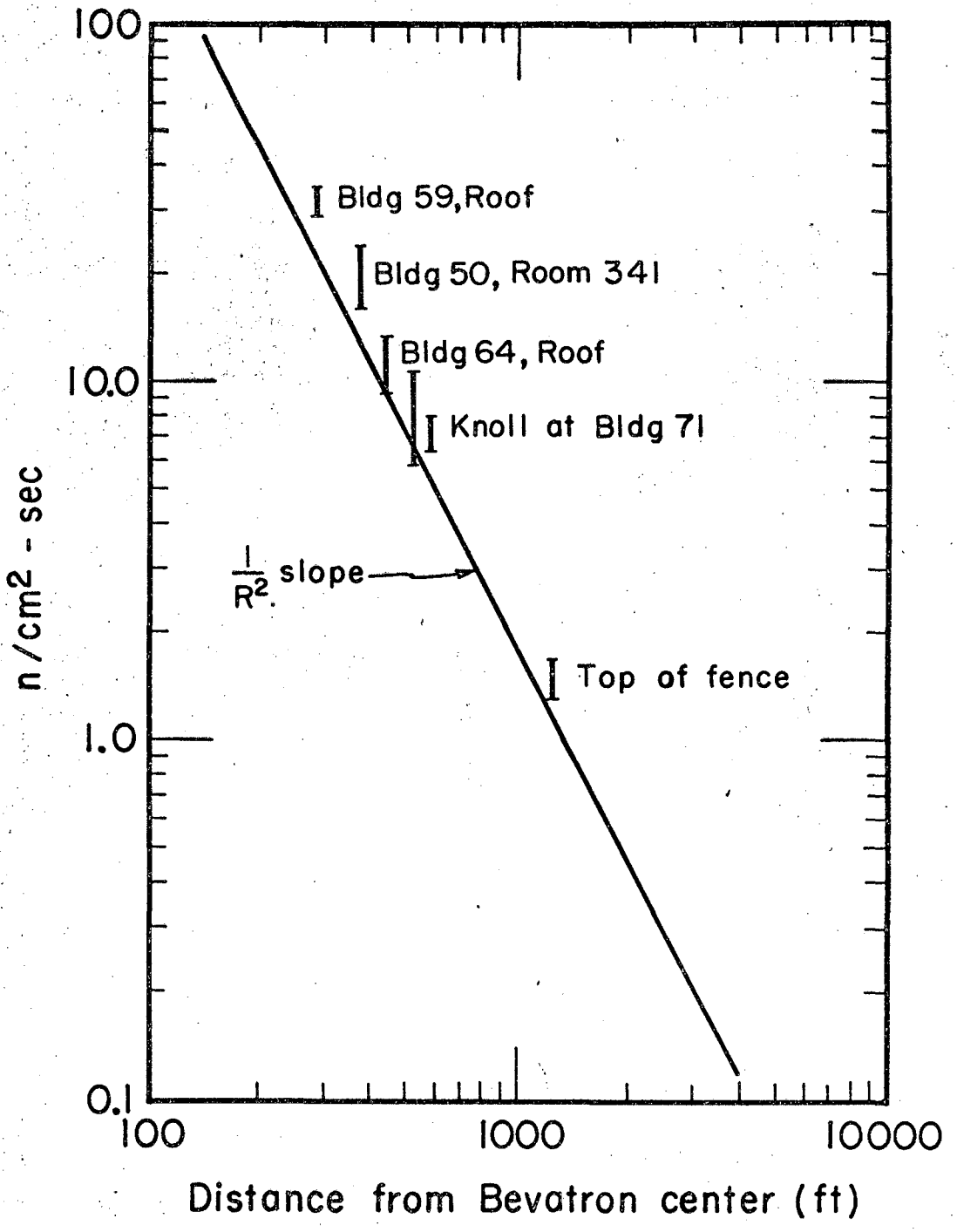

MU-25960

UCRL-10086
Fig. 12

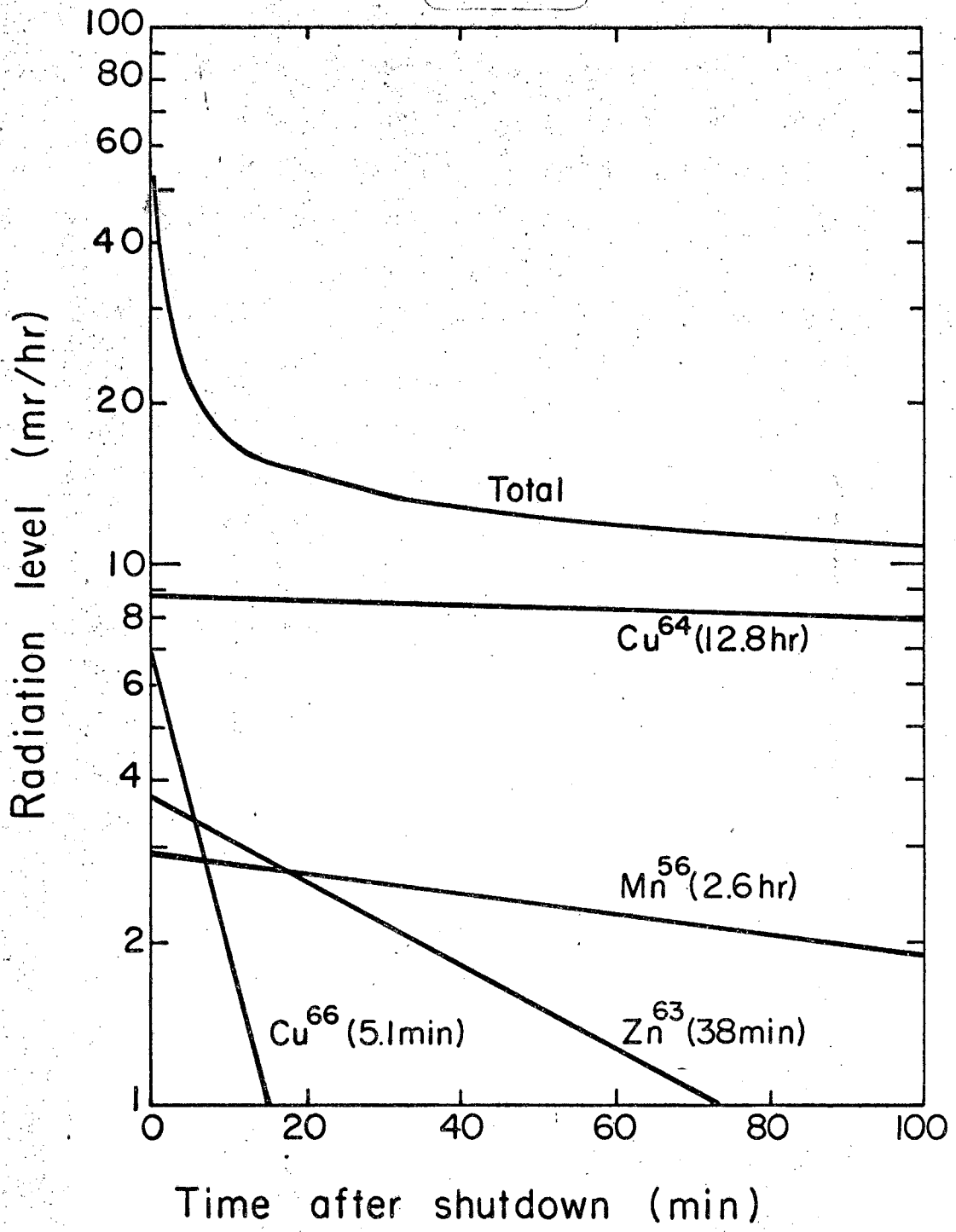

MU-26630
UCRL-10086
Fig.13

TABLE I

Secondary particle production, residual nuclear excitation and temperature for aluminum targets in the beam of three meson-factory accelerators.

Proton energy (MeV)	Total neutron Thick Al target yield(n/p)	Total* No. cascade nucleons per incident proton on Al	No. cascade* neutrons per incident proton on Al	No. cascade* protons per incident proton on Al	Residual* nuclear excitation E_1(MeV)	Residual* nuclear temperature τ(MeV)	No. evaporation neutrons per incident neutron or proton
450	1.3	3.12	1.27	1.85	63	4.3	1.08
600	2.0	3.40	1.35	2.05	72	4.5	1.12
850	3.9	3.70	1.45	2.25	88	4.9	1.17

*See ref. 4.

TABLE 2

N atoms/cm^3 for Berkeley concrete($\times 10^{22}$).

O	4.73
H	1.73
Si	1.57
Ca	0.26
Al	0.17
Fe	0.053
Na	0.028
K	0.028
Mg	0.013

TABLE 3

Assumed relation between σ_a, the neutron attenuation cross section, and σ_{tot}, the total neutron cross section.

(MeV)	
1	$\sigma_a = 1.00\ \sigma_{tot}$
5	$\sigma_a = 0.65\ \sigma_{tot}$
14	$\sigma_a = 0.055\ \sigma_{tot}$
≥150	$\sigma_a = 0.50\ \sigma_{tot}$

TABLE 4

$N\sigma_a(cm^{-1})$ for various elements ($\times 10^{-2}$)

	1 MeV	14 MeV	270 MeV
O	16	4.4	0.89
H	7.8	0.64	0.026
Si	4.7	1.7	0.41
Ca	0.78	0.33	0.10
Al	0.51	0.16	0.05
Fe	0.16	0.045	0.028

TABLE 5

Estimate of neutron and proton emission from cascade and evaporation processes per collision induced in inelastic collisions of neutrons of energy E_n with nuclei of atomic weight near $A = 20$ (Ne). (E_1 and τ are, respectively, the excitation and "temperature" of the residual nuclei following the cascade. *)

	E_n =	50	100	2000	500	1000	2000	MeV
	p/n	0.4	0.6	0.9	1.2	1.5	1.9	
Cascade	n/n	0.7	1.2	1.5	2.0	2.4	3.1	
	E_1	27	35	37	40	53	72	MeV
	τ	3.7	4.2	4.3	4.5	5.2	6.0	MeV
	p/n	0.7	0.8	0.9	1.0	1.0	1.3	
Evaporation	n/n	1.0	1.0	1.0	1.1	1.2	1.5	

*See ref. 4).

TABLE 6

Estimate of neutron and proton emission from cascade processes induced per nuclear collision by inelastic collisions of protons of energy E_n with nuclei of atomic number near A = 20 (Ne). (E_1 and τ are respectively the excitation and "temperature" of the residual nuclei following the cascade.*)

	E_n =	50	100	200	500	1000	2000	
Cascade	p/p	0.6	1.0	1.4	1.9	2.4	3.2	
	n/p	0.5	0.8	1.0	1.3	1.5	1.8	
π^*/p		0	0	0	0.1	0.4	1.0	
	E_1	27	35	37	40	53	72	MeV
	τ	3.7	4.2	4.3	4.5	5.2	6.0	MeV
Evaporation	p/p	0.7	0.8	0.9	1.0	1.0	1.3	
	n/p	1.0	1.0	1.0	1.1	1.2	1.5	
	H^2/p	0.1	0.1	0.1	0.2	0.3	0.5	
	H^3/p	0.02	0.02	0.02	0.04	0.05	0.07	
	He^3/p	0.03	0.03	0.04	0.06	0.08	0.1	
	He^4/p	0.2	0.3	0.4	0.5	0.6	1.0	
	Li, Be, C, etc./p	—	~~0.06~~	0.05	0.1	0.1	0.1	

*See ref. 4).

TABLE 7

Estimate of neutron and proton emission from cascade processes induced per nuclear collision by inelastic collisions of protons of energy E_n with nuclei of atomic number near A = 60 (Ni). (E_1 and τ are respectively the excitation and "temperature" of the residual nuclei following the cascade. *)

	E_n	50	100	200	500	1000	2000	MeV
Cascade	p/p	0.3	0.7	1.0	1.8	2.7	4.2	
	n/p	0.4	0.7	1.1	1.7	2.6	4.0	
	$\pi^{\pm}$/p	0	0	0	0.1	0.4	1.0	
	E_1	39	49	58	85	130	202	MeV
	τ	2.5	2.9	3.1	3.8	4.7	5.8	MeV
Evaporation	p/p	0.5	0.6	0.7	1.1	1.8	2.6	
	n/p	2.0	2.4	2.7	3.6	4.4	5.3	
	H^2/p	0	0.02	0.02	0.04	0.4	0.8	
	H^3/p	0	0	0	0	0.01	0.02	
	He^3/p	0	0	0.01	0.02	0.02	0.03	
	He^4/p	0.1	0.1	0.2	0.2	0.4	0.7	
	Li, Be, C, etc./p	0	0	0.01	0.02	0.03	0.05	

TABLE 8

Mean free paths in air

E neutron (MeV)	$\lambda_{collision}$ (m)	λ_{tr} (m)	λ_a (m)	$\sqrt{\lambda_a \lambda_{tr}/3}$ (m)
150	740	—	—	—
50	185	—	—	—
20	120	—	—	—
1	92	100	1840	250

TABLE 9

Neutrons/incident accelerated particle striking a copper target

Energy (MeV)	Particle	n/particle
340	p	1.5
450	p	2.0
600	p	3.3
730	p	6.4
850	p	7.0
450	d	2.0
900	α	4.0
1100	He^3	6.1